PROCEEDINGS OF SPIE

SPIEDigitalLibrary.org/conference-proceedings-of-spie

Experimental investigation of high-power laser irradiation of missile materials in subsonic and supersonic flows

Sebastian Schäffer, Dirk Allofs, Patrick Gruhn, Ali Gülhan, Martin Lueck, et al.

Sebastian Schäffer, Dirk Allofs, Patrick Gruhn, Ali Gülhan, Martin Lueck, Jens Osterholz, "Experimental investigation of high-power laser irradiation of missile materials in subsonic and supersonic flows," Proc. SPIE 12273, High-Power Lasers and Technologies for Optical Countermeasures, 122730M (2 November 2022); doi: 10.1117/12.2647841

SPIE.

Event: SPIE Security + Defence, 2022, Berlin, Germany

Experimental investigation of high-power laser irradiation of missile materials in subsonic and supersonic flows

Sebastian Schäffer[a], Dirk Allofs[b], Patrick Gruhn[b], Ali Gülhan[b], Martin Lueck*[a], Jens Osterholz[a]
[a]Fraunhofer Institute for High-Speed Dynamics, Ernst-Mach-Institut, EMI, Ernst-Zermelo-Straße 4, 79104 Freiburg, Germany; [b]DLR, German Aerospace Center, 51147 Cologne, Germany

ABSTRACT

The technology of missiles and of their countermeasures is evolving continuously. High-power lasers are an option to encounter these threats. In order to understand their potential in such a scenario, it is vital to investigate the laser effects in the presence of a corresponding aerodynamic environment. Thus, experimental and numerical investigations were conducted cooperatively by Fraunhofer Ernst-Mach-Institut and the Supersonic and Hypersonic Technologies Department of DLR. An ytterbium fiber laser system was installed at the supersonic wind tunnel VMK. The laboratory was fit to meet necessary laser safety requirements. Combined subsonic and supersonic flow and high-power laser experiments with flow velocities up to a Mach number of 3 and a laser power up to 10 kW were realized. Two kind of tests were performed, focusing on laser beam distortion through aero-optical effects and on high-power laser effects, respectively. The interaction effects between aerodynamics, laser radiation and irradiated targets were studied on flat-plates as well as cylindrical and radome targets, simulating generic missile design. Irradiated objects consisted of steel, aluminum, carbon-fiber-reinforced polymer and the ceramic-based composite WHIPOX. While beam distortions were studied with a wavefront sensor, damaging processes were investigated by measuring the perforation time of the targets, as well as via high-speed imaging, thermography as well as Schlieren imaging. Numerical three-dimensional, steady, and uncoupled simulations were performed. The data indicated complex interactions between material, laser beam, and aerodynamics. This investigation can be used as an initial basis for further analysis of laser-material-aerodynamic interactions with respect to missile defense.

Keywords: Laser effects, perforation, aero-optics, wind tunnel, subsonic, supersonic, Schlieren, missile defense

1. INTRODUCTION

The interest in optical countermeasures has grown significantly in recent years because of further development of high-performance laser systems. Furthermore, the missile technology is constantly evolving with respect to the use of novel materials and propulsion technology. This becomes particularly apparent in the field of hypersonic missiles, which are currently in development by various nations [1][2]. High-power lasers are an option to encounter such threats [3]. Since missiles can achieve supersonic and hypersonic Mach numbers, the applicable interaction time is in the range of seconds. Therefore, it is vital to understand basic effects and interaction mechanisms that are relevant for the defense against missiles using a laser effector. In general, a flying target that is subjected to laser radiation undergoes complex laser-material-aerodynamic interactions, involving a local temperature rise that can result in structure modifications like material ablation or melt removal, additionally boosted by the airflow. Johnson et al. as well as Robin et al. promoted a reduction of laser melt-through time due to a transverse gas flow [4][5]. They developed simplified models for an analytical description of the coupling behavior of laser, gas flow and molten material to predict the perforation time as a function of gas flow velocity and power density of the laser. Crane et al. studied the ablation of metals subjected to a CO_2 laser and a tangential subsonic gas flow [6]. The experimental results showed a linear relationship between the ablation rate and the incident laser power density while the surface temperature remained almost constant. The melt was assumed to be removed by the aerodynamic shear stress. Moreover, oxidation processes of the metal surface were observed to have a major influence on the absorptance of the laser. Baek et al. and Wei et al. irradiated metal samples with a 1.07 µm cw laser and studied the melt-through characteristics in flow speeds up to 90 m/s [7][8]. In addition to a reduced perforation time by the gas flow, Baek et al. determined threshold irradiances in dependence of material thickness and beam absorptivity.

*martin.lueck@emi.fraunhofer.de; phone +49 761 2714 407; emi.fraunhofer.de

High-Power Lasers and Technologies for Optical Countermeasures, edited by David H. Titterton, Robert J. Grasso, Harro Ackermann, Willy L. Bohn, Mark A. Richardson, Proc. of SPIE Vol. 12273, 122730M
© 2022 SPIE · 0277-786X · doi: 10.1117/12.2647841

In recent years, research has been carried out on the damage effect of composite structures in a supersonic airflow. Wang et al. investigated the laser ablation of C/SiC composites exposed to a 2 kW cw laser operating at 1.07 µm in an airflow at a Mach number of 2 [9]. According to their results, ablation rates of C/SiC composites were increased due to the supersonic airflow. In addition, the surface morphology of the irradiated area differed significantly from samples that were exposed to the laser beam under static air conditions. Due to convective cooling the outer regions of the irradiated zone were less damaged. Zhao et al. conducted an experimental study on laser ablation of laminated CFRP that was subjected to a tangential supersonic airflow at a Mach number of 3 [10]. They identified two regions with different ablation morphologies, a coupled ablation zone in the vicinity of the point of laser impact and a heat-affected zone in the direction of the airflow. They investigated the ablation behavior under four other flow environments and found that thermo-mechanical erosion due to a tangential supersonic flow plays a significant role in the laser ablation process.

This paper gives an overview of a joint research program of Fraunhofer EMI and DLR that involved high-power laser experiments in a steady subsonic and supersonic flow at the Supersonic and Hypersonic Technologies Department of DLR. The purpose of the test campaign was to demonstrate the ability of a DLR wind tunnel facility to conduct high-power laser experiments in subsonic and supersonic flows, and to gather fundamental, experimental and numerical data regarding laser irradiation-aerodynamic-material interactions. The highlights of the presented experiments are significantly longer test times of up to 30 s in supersonic flows, compared to above mentioned studies, where laser irradiation experiments with a duration of several seconds were conducted mainly under subsonic flow conditions.

The experimental series can be divided into two parts. The first part focused on aero-optics affecting laser propagation. Turbulent flows, boundary layers, and other supersonic flow phenomena result in density variations within the flow field. Thereby, the refractive index is varying locally, which causes optical distortion of a propagating beam [11]. These aero-optical effects were studied by means of a low-power laser and a wavefront sensor (see section 2.4).

The second part of the investigations focused on laser-matter interaction. The material and parameter selection were oriented on previous experimental studies carried out at Fraunhofer EMI including laser irradiations with laser powers up to 10 kW [12][13]. Furthermore, the selected test materials as well as the generic geometries of the models were also considered to be representative for corresponding missile threat scenarios. The generic model shapes simplified the numerical calculations. These simulations of unperforated and perforated test targets were performed to separate the effects of boundary layer heating and geometry changes on aerodynamics.

The agenda of this work is as follows: First, the wind tunnel facility and the measurement setups for both experimental parts are described and the target material selection is explained. Afterwards, results of the implemented measurement techniques are discussed and the numerical simulations are explained. Finally, a conclusion about the test campaign is given.

2. EXPERIMENTAL SETUP

2.1 Wind tunnel facility VMK

The experiments were performed at the Supersonic and Hypersonic Technologies Department of DLR. Due to the high-power laser radiation, special laser safety precautions were required. These requirements could be best accomplished in the Vertikale Messstrecke Köln (VMK) wind tunnel facility. This facility was originally built for investigations of air-breathing engines and propellant testing. An 11 m high tower made of concrete surrounds the vertically directed free stream measurement section. A facility silencer is placed on top of the tower, to allow testing without significant noise disturbance for the environment. The measurement room with a ground area of 4 x 4 m^2 offered enough space for the installation of the laser optics and measurement equipment.

The VMK is a blow-down wind tunnel facility, using high-pressurized air from reservoir tanks. Due to the capacity of the tanks, it is possible to realize supersonic flows up to Mach 3 for about 30 seconds. The maximum total pressure p_0 is up to 65 bar, while the maximum achievable total temperature T_0 is up to 750 K. Subsonic and supersonic flows in the range of Mach number between 0.5 and 3.0 can be achieved by different nozzle geometries. The unit Reynolds number Re_∞ ranges from 5e6 to 3e8 1/m. In this study, two specific flow conditions were set for the investigations, which are summarized in Table 1. The temperature T is the static temperature within the flow.

For supersonic flows, a nozzle extension was used to avoid laser beam distortion by the nozzle's boundary layer. Within this extension, a glass window was placed. No nozzle extension was available for the subsonic nozzle.

Table 1. VMK test conditions

run type	Ma [-]	d_{nozzle} [mm]	T_0 [K]	T [K]	p_0 [bar]	Re_∞ [1/m]
subsonic	0.8	340	289	256	1.597	2.3e7
supersonic	3	312	282-291	101-104	20.95	1.7e8

A comprehensive risk assessment considering laser safety was conducted. In that framework, the VMK was equipped with an advanced interlock system, special housings for the Schlieren measurement system, IR-sensitive monitoring cameras, and visual covers between concrete tower and facility silencer. Because the VMK is close to the airport Cologne-Bonn, a temporal flight restriction 50 m around the VMK building was commissioned. Behind the irradiated targets, multiple beam dumps made of aluminum were placed. By means of manual beam propagation calculations, it was controlled that beam reflections were only directed to additional installed beam dumps within the concrete tower. A photodiode was set up for automatic shut-down of the laser system as soon as the target was perforated.

2.2 Wind Tunnel Models

Three types of models were manufactured: a flat-plate model, a cylindrical model and a radome model. All three models are depicted in Figure 1. Here, the irradiated target sample is marked red and the safety absorber made of aluminum is marked yellow. The flat plate-model had a hollow model mount (marked green), allowing the analysis of the undeflected laser beam by means of e.g. a wavefront sensor, which could be placed in the blue-marked box. For these tests, the aluminum absorber was removed and the target sample was replaced by a borofloat window. As a consequence, the flat-plate model could be used for generic aero-optical and irradiation testing, while the cylindrical and the radome model were only used for irradiation tests. The geometry of the cylindrical and radome targets was derived from generic missile design.

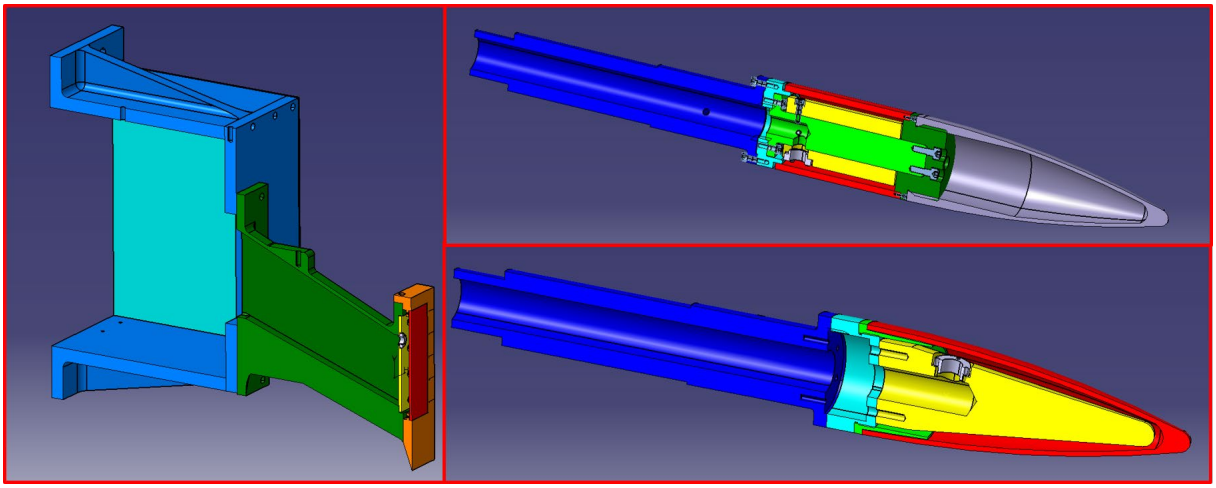

Figure 1. Model designs, left: flat-plate model, top right: cylindrical model, bottom right: radome model

2.3 Materials

The irradiated flat-plate samples possessed a thickness of 5 mm and were made of four different materials including S235 steel, aluminum with a purity of 99.0 %, carbon-fiber-reinforced polymer (CFRP) and wound highly porous oxide composite (WHIPOX). The CFRP is an epoxy-based composite with a unidirectional layup design of 0°/90°. The CFRP laminates were manufactured with a commercial fabric prepreg wrapping technology. The percentage of fibers was approx. 55%. The surface of the flat-plate samples had a typical carbon textural structure. WHIPOX is a fiber-reinforced

oxide ceramic composite that was developed by DLR for high-temperature applications in aerospace and energy engineering [14]. The composite contains parts of aluminum oxide and features a high thermo-shock resistance.

The materials selection was derived from previous experimental studies carried out at Fraunhofer EMI irradiating materials like metals and fiber-reinforced composites with laser powers up to 10 kW [12][13]. The special oxide ceramic composite WHIPOX was incorporated in the test series as a representative material for supersonic missile applications.

2.4 Aero-optic related experiments

For the analysis of beam distortions and aberrations the wind tunnel served as an aero-optical environment, where the laser was placed outside the flow field and the laser beam was directed onto a wavefront sensor housed inside a model in the air stream. This setup enabled the investigation of aerodynamically induced density variations that affected the laser beam before it hit the target.

The experimental setup for aero-optical tests is illustrated in Figure 2. A low-power single-mode laser (Spectra-Physics Excelsior) with a wavelength of 1064 nm was mounted on a platform next to the air nozzle. The laser power was adjusted using neutral-density (ND) filters. The angle of incidence was adjusted to approx. 60° between laser beam and model surface. The flat-plate model was installed close to the exit of the air nozzle in order to have the target fully submerged inside the nozzle's Mach cone, in which flow conditions are constant. Geometric properties of supersonic flow experiments can be taken from the right-hand side of Figure 2. For the aero-optical tests, a borofloat window was mounted at the flat-plate model. The wavefront sensor was placed inside the box of the flat-plate model holder. The sectional view in Figure 1 shows the optical path from the laser to the wavefront sensor.

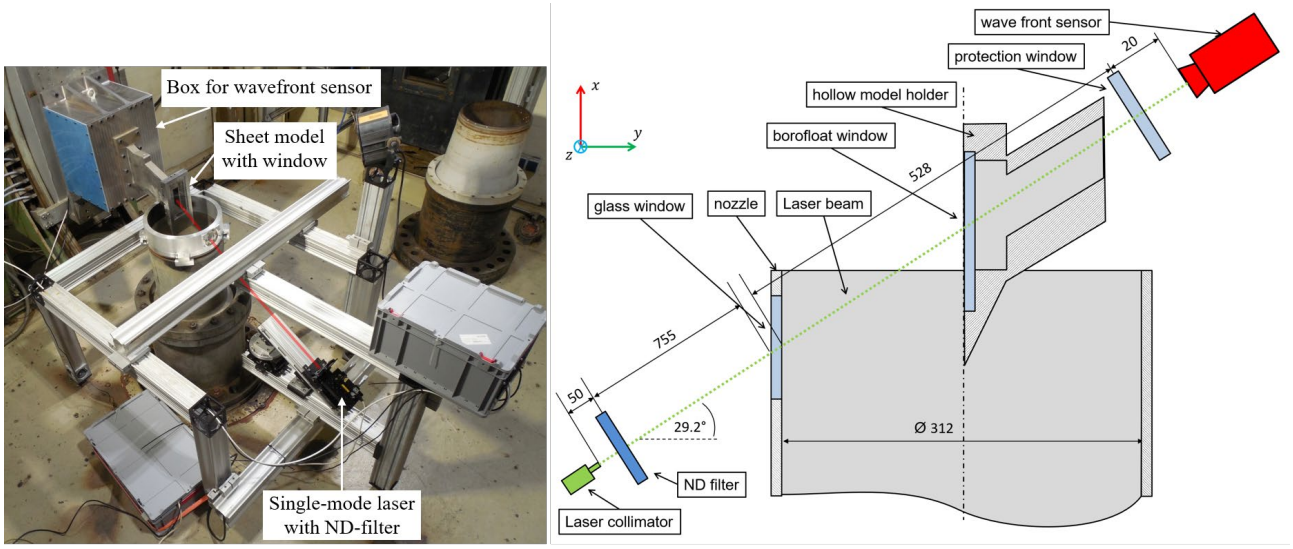

Figure 2. Experimental setup of the aero-optical experiments with low-power laser and wavefront sensor.

Intensity and phase imaging of the impinged laser beam were measured using a quadri-wave lateral shearing interferometer (Phasics SID4-HR). This technique is based on a modified Shack-Hartmann mask, but it features a four times higher lateral resolution, an improved signal-to-noise ratio and a high dynamic range (500 µm peak-to-valley) compared to a conventional Shack-Hartmann wavefront sensor [15].

2.5 High-power laser experiments

For the high-power laser tests various imaging methods were utilized to study the dynamics of the laser-matter interaction during the experiment. The setup of an irradiation experiment with a cylindrical target is illustrated in Figure 3. The low-power laser was exchanged with a collimator of the high-power laser system. An ytterbium fiber laser with a wavelength of 1070 nm and a cw output power of 10 kW was installed. The collimated beam had a Gaussian intensity distribution with a beam diameter of about 11 mm. Above the laser mount an infrared microbolometer (FLIR A655sc) was positioned to record the heated target surface with a frame rate of 50 fps. It was encased inside a box for safety reasons. A high-speed camera (Phantom v1610) was placed outside the wind tunnel and observed the interaction

zone through a glass window. Additional illumination allowed for frame rates of about 2000 fps. In addition, a Schlieren imaging system was used to visualize the airflow around the target with a frame rate of about 60 fps. The perforation time was measured using a photodiode that was mounted inside the model behind the target. Once the photodiode detected laser light, an electronic control device terminated the laser irradiation within a few milliseconds.

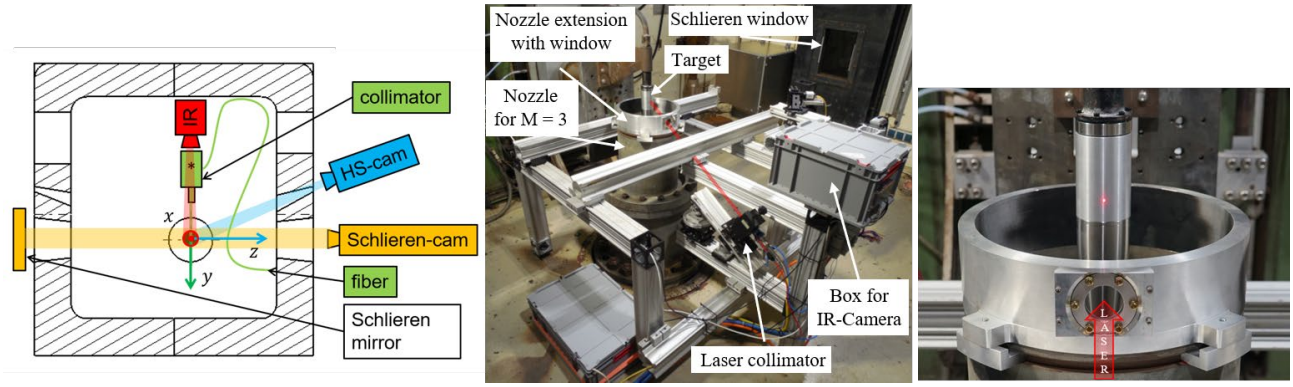

Figure 3. Experimental setup for irradiation of missile material in supersonic wind tunnel VMK.

3. RESULTS AND DISCUSSION

3.1 Aero-optical measurements

In the following, the results of the aero-optical laser beam propagation measurements are discussed. The VMK generated intense vibrations during supersonic flow that were transmitted to the platforms of the laser and of the wavefront sensor. These vibrations were challenging for an appropriate mounting of both the wavefront sensor and the low-power single-mode laser and the respective analysis. Despite this limitation several measurements during a test period of 30 seconds under the influence of subsonic and supersonic flow conditions were conducted. The interferometry measurement offers quantitative phase imaging to estimate the deformations of the wavefront by measuring the optical path difference. The results show that wavefront distortions are significantly increased when establishing a surrounding flow field. Wavefront errors were analyzed by determining the Zernike coefficients of the aberrated wavefront suggesting a predominantly impact of piston and tip-tilt errors. In addition, a deflection of the laser beam was observed on the wavefront sensor. Figure 4 exemplarily shows intensity profiles during an experiment with a supersonic flow at Mach 3.

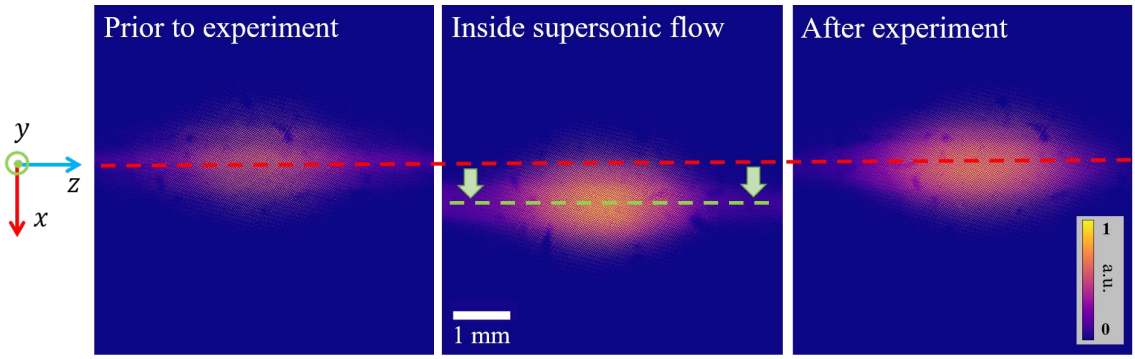

Figure 4. Intensity profiles of wavefront sensor measurements during a supersonic flow experiment at Mach 3 indicating a local beam deflection in negative x-direction (cf. Figure 2).

A reproducible lateral offset of 0.74 mm inclined downward on the CCD-chip of the wavefront sensor was observed during supersonic flow. This local shift is assumed to be caused by beam diffraction either at the Mach wave that spread

upward from the front tip of the flat-plate model, or at the nozzle's boundary layer. This hypothesis must be tested in further investigations.

3.2 High-power laser irradiation of missile materials

For the irradiation experiments of missile materials, the laser was operated at 5 to 10 kW. Every investigated material exhibited a different process dynamic when the laser hit the target in the presence of a steady aerodynamic environment. The interaction effects between aerodynamics, laser radiation, and irradiated targets can be observed via high-speed imaging, illustrated in Figure 5. All pictured samples were irradiated with a laser power of 10 kW in a supersonic flow at Mach 3 The steel plate (cf. left-hand side in Figure 5) exhibited the fasted perforation of all tested materials after about 0.7 s at maximum laser power at subsonic and supersonic flow velocities. Melting and emitting sparks could already be observed within a few milliseconds of laser irradiation. The molten material was effectively removed from the melt pool.

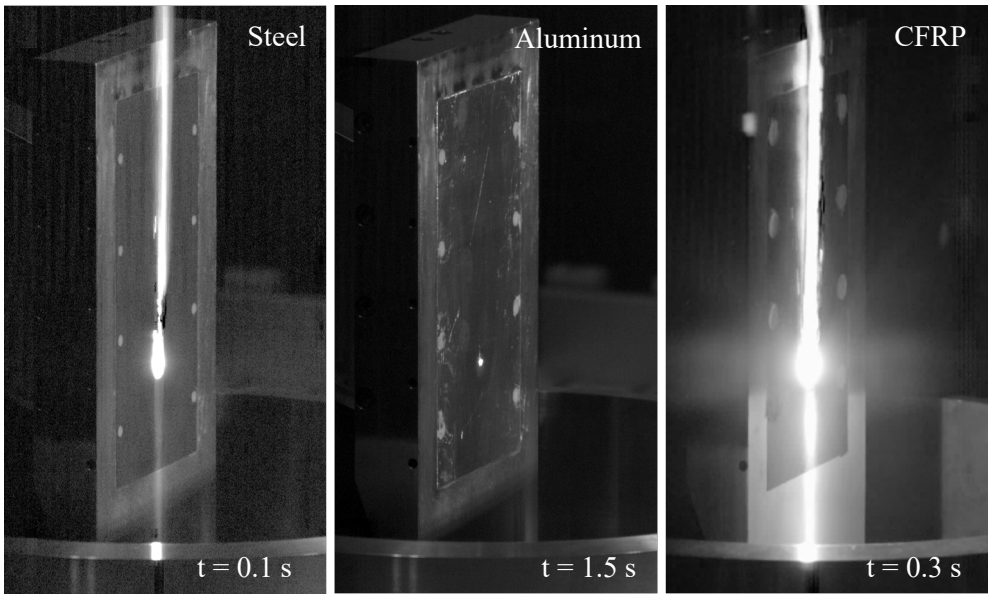

Figure 5. Snapshots from irradiation experiments with flat plate model and different materials. From left to right: steel, aluminum, CFRP. All targets were irradiated with a laser power of 10 kW and a beam diameter of 11 mm. Flow Mach number was 3.

Regarding aluminum targets, no surface modification was visible for a laser power of 5 kW. With a laser power of 10 kW, a delayed melting after an irradiation time of about 1.2 s and a total perforation time of 3-4 s was determined, depending on the flow velocity. Since aluminum offers a comparatively high reflectivity and thermal conductivity, it took a certain amount of time to absorb sufficient laser energy before melting started. For further investigation of this threshold effect an additional laser power of 7.5 kW was tested under subsonic conditions. The aluminum plate was melted at this power level and the perforation time was twice as high as at a laser power of 10 kW.

After the melting process started, little melt droplets were carried along with the airstream. However, parts of the molten aluminum remained at the melt pool due to its surface tension. After further irradiation, more molten material became entrained in the airflow in a piecewise manner. Subsequent to perforation, the photodiode detected the laser light, and the laser irradiation was automatically stopped within a few milliseconds. Due to this sudden stop the exit holes on the rear sides collectively appeared to be small (Ø ~ 1-2 mm) compared to the entry holes at the front surfaces (Ø ~ 10-20 mm).

High-speed video images of the irradiation of the CFRP plate demonstrated that the damage process began only a few milliseconds after the laser beam hit the composite target. This included decomposition of the epoxy matrix and ablation of CFRP fragments visible in the smoke cloud. The irradiation of the CFRP resulted in a bright reaction region that was blown downstream.

To analyze the influence of aerodynamics on the perforation time, also laser irradiation tests of the flat-plate targets made of steel, aluminum and CFRP in a no-flow environment were conducted. Figure 6 exemplarily summarizes the

experimental results for the determined perforation times of irradiated aluminum, steel and CFRP plates under different flow conditions. In general, the higher the laser power, the shorter the perforation time. For CFRP material, a minor correlation of the perforation times could be observed with respect to the applied flow conditions, i.e. the higher the flow velocity the faster the perforation (cf. Figure 6). This correlation can be explained by the fact that the process plume in front of the plate is removed by the continuous air stream as known from previous studies [16]. The perforation time of flat plates made of steel were shortened by the factor of three in subsonic and supersonic flow, compared to the static environment. However, no significant difference of the perforation time in subsonic or supersonic flow could be seen. On the other hand, aluminum showed a similar behavior for a static as well as for an aerodynamic environment. A similar threshold effect and similar perforation times were observed, leading to the assumption that the influence of a surrounding airflow on that threshold can be neglected for the investigated range of flow velocities.

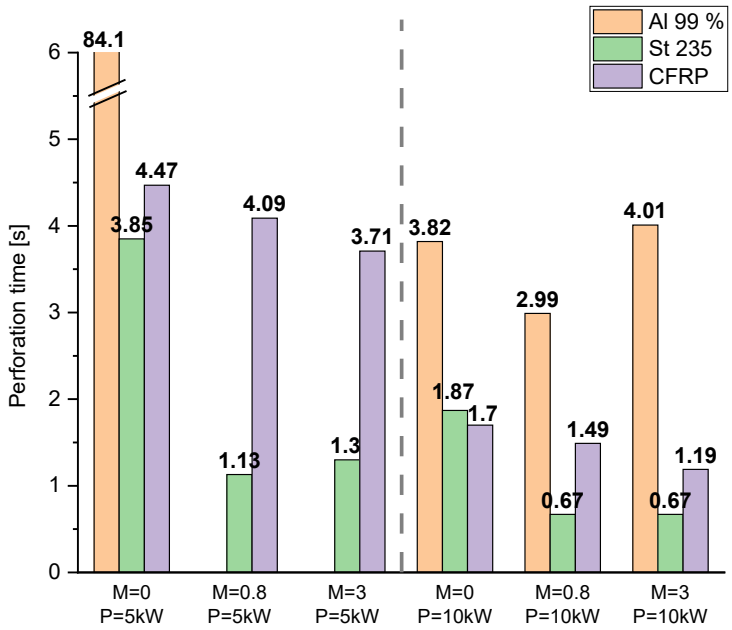

Figure 6. Perforation times for the irradiation of aluminum, steel and CFRP plates with a thickness of 5 mm with different airflow conditions (Mach number 0 to 3).

Damages of the irradiated missile materials are illustrated in Figure 7. The depicted targets correspond to the experiments represented by the high-speed images of Figure 5. The steel plate showed a hemispherical damage at the point of laser impact. Compared to steel, the damage zone of the aluminum targets has a rougher appearance. Liquified material from the melt pool was either entrained in the airflow or partly attached downstream of the melt pool indicated by a fan-shaped solidified melt. This characteristic could be observed for both the aluminum and steel targets.

Based on the visual inspection of the irradiated CFRP plate, the damaged area can be divided into two regions, a cone-shaped ablation zone and a heat-affected zone downstream on the surface. At the center of the laser spot the resin matrix and carbon fibers were ablated. The airflow effectively removed the ablated material resulting in a cone-shaped penetration channel. The area outside of the laser spot is nonetheless affected by the absorbed heat and the hot CFRP residuals blown downstream. This becomes apparent by revealed carbon fibers and the decomposed epoxy matrix. Due to their thermal stability, the carbon fibers were mostly unaffected in their structure, while the epoxy resin was decomposed, as known from previous studies [12]. In addition, CFRP layers were ablated incrementally resulting in a sharply confined and conically shaped penetration channel.

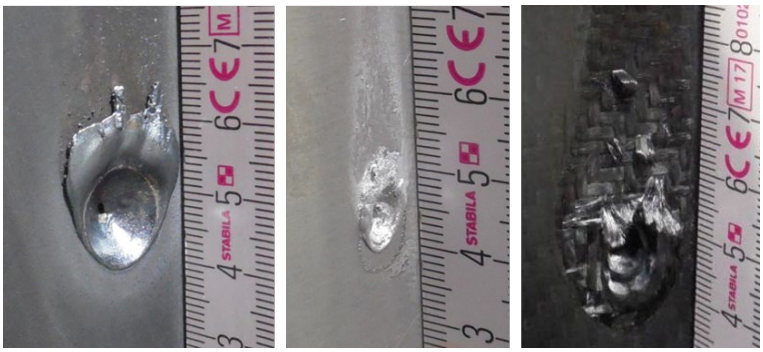

Figure 7. Damage of missile materials steel, aluminum and CFRP after laser irradiation. All targets were irradiated with a laser power of 10 kW and a beam diameter of 11 mm. Flow velocities were at Mach 3.

An irradiation experiment with the WHIPOX was conducted with a laser power of 10 kW in a subsonic flow at Mach 0.8. Contrary to expectations associated with a high heat resistance, WHIPOX inflamed already after a laser exposure time of 0.3 s. A snapshot of this moment is visualized in Figure 8 showing melting of the oxide matrix and an additional ablation of fiber material. From the visual inspection of irradiated WHIPOX a material transformation is apparent. The oxide ceramic composite was rather melted than ablated as a consequence of laser irradiation. It is assumed that the brown color of the melted WHIPOX comes from tiny rust particles within the flow or emerging material transformations that resulted in the formation of corundum (fused aluminum oxide).

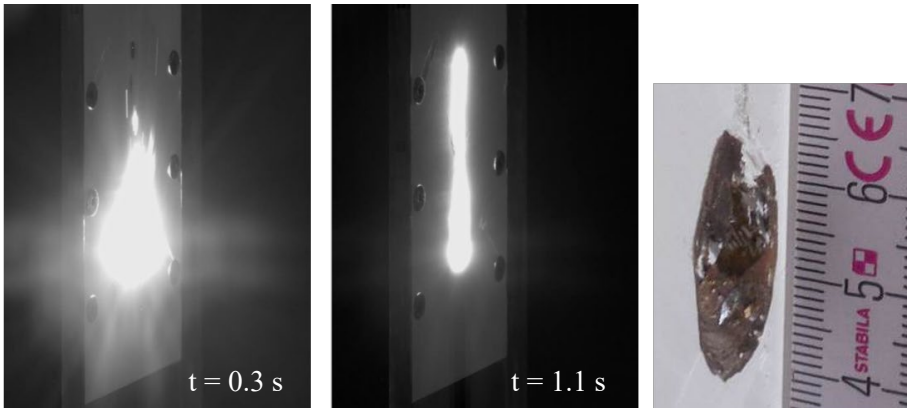

Figure 8. Laser irradiation of WHIPOX plate with a laser power of 10 kW at Mach 0.8 and damage after experiment.

An infrared camera measured the radiant heat emitted by the targets in order to investigate the surface temperature of missile material during laser irradiation experiments. Laser irradiation and thermography experiments with CFRP and WHIPOX composites demonstrated that the current setup of a long-wave infrared camera with a spectral range from 7 to 14 µm is not suited for such materials. Very hot particles and fibers caused a prompt overexposure of the infrared camera sensor even at the highest calibration range up to 2000 °C. Hence, thermography results were restricted to laser irradiation of metal samples. Figure 9 exemplarily shows a temperature profile of an aluminum cylinder that was irradiated with a laser power of 10 kW and a beam diameter of 11 mm in a supersonic flow at Mach 3. The infrared camera needs a preset emissivity to calculate temperatures on the basis of the detected radiant flux. For the presented aluminum cylinder, the emissivity was set to $\varepsilon = 0.3$, representing aluminum with a slightly roughened surface [17]. The selected calibration of the camera covered a temperature range of 100 to 650 °C. Subsequent to laser activation, a temperature rise was observable until an indentation at about 550 °C after 0.6 s. This moment can be associated with a phase-change when the aluminum surface started to melt. The deviation to an expected melting temperature above 600 °C can be explained by uncertainties of the emissivity and potential chemical reactions like oxidation. Images of the high-speed camera showed surface modifications of the aluminum surface in the center of the laser spot after 0.6 s, which confirmed the begin of the melting process (cf. Figure 9 right-hand side). Accordingly, thermography signals can help with the interpretation of transformation processes during high-power laser melting.

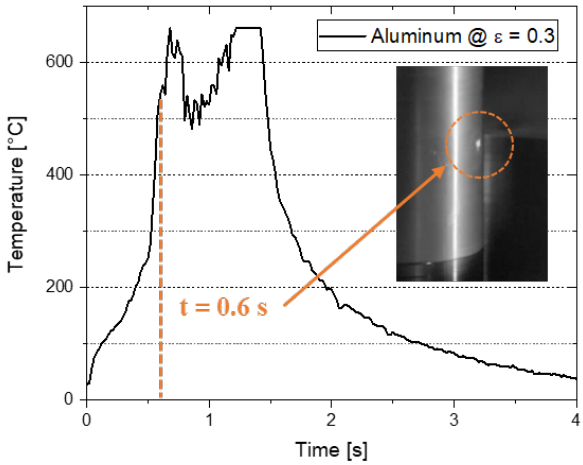

Figure 9. Surface temperature of an aluminum cylinder at the area of laser impact when applying a laser power of 10 kW and a supersonic flow at Mach 3.

Schlieren imaging was used to investigate disturbances of the flow around the target during the laser irradiation. An example of Schlieren image of a cylindrical model made of alumina at Mach 3, before and after laser radiation, is given in Figure 10. The black bar on the left-hand side is the shadow, produced by the cylindrical model. The surface distortion, caused by the laser radiation, is clearly visible in the image on the right. Mach waves were generated at the edges of those surface distortions. However, neither a flow separation nor a boundary layer transition can be detected, which are assumed to have major effects on aerodynamic forces.

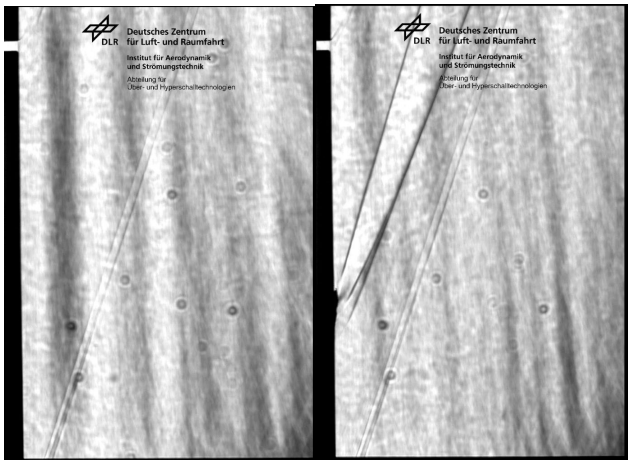

Figure 10. Schlieren image of aluminum cylinder at Mach 3 before and after laser irradiation with a laser power of 10 kW.

3.3 Numerical simulations of irradiated plate models

Numerical simulations were conducted in order to answer the question whether the aerodynamics around the irradiated targets were considerably distorted. Aerodynamic distortions could have a significant impact on e.g. the aerodynamic stability of flying missiles.

Three-dimensional simulations were performed with the DLR Tau code, which is a finite-volume flow solver [18][19]. For turbulence modelling, the SST model by Menter was implemented [20]. To reduce computational costs, flow and model domain were split at the symmetry plane. Simulations included interactions between model surface and flow; laser radiation was neglected. Four test cases in the supersonic flow were simulated:

1. Cold, unperforated plate model
2. Unperforated plate model with thermal hotspot
3. Cold, perforated plate model
4. Perforated plate model with thermal hotspot

The four test cases allow to separately analyze the impact of the thermal heating caused by laser irradiation and of the surface damage caused by the perforation. It was attempted to reproduce the perforation geometry from irradiated plate models made of steel. A hemispherically shaped immersion of 12 mm in diameter and a 1 mm high elevation, which is located directly behind the immersion, simulate the irradiated plate geometry. While the immersion came from the melting process, the elevation grew from molten material out of the immersion, which solidified. See the cross section in Figure 11 for illustration. In case 2, a spot of 11 mm in diameter on the plate surface was defined to have a temperature of 2000 K. In case 4, this temperature was set to the surface of the immersion, while the elevation's surface temperature was set to 1000 K.

The numerical comparison showed that only for cases, in which the perforated model was simulated (case 3 and 4), slight impacts on the aerodynamics were observed. Since neither a boundary layer transition nor a separation occurred, the authors assumed that the impact of the final perforation and thermal surface heating on aerodynamic stability could be neglected. It must be noted that the simulations did not consider effects during the material melting. Further analyses are required to support a final conclusion.

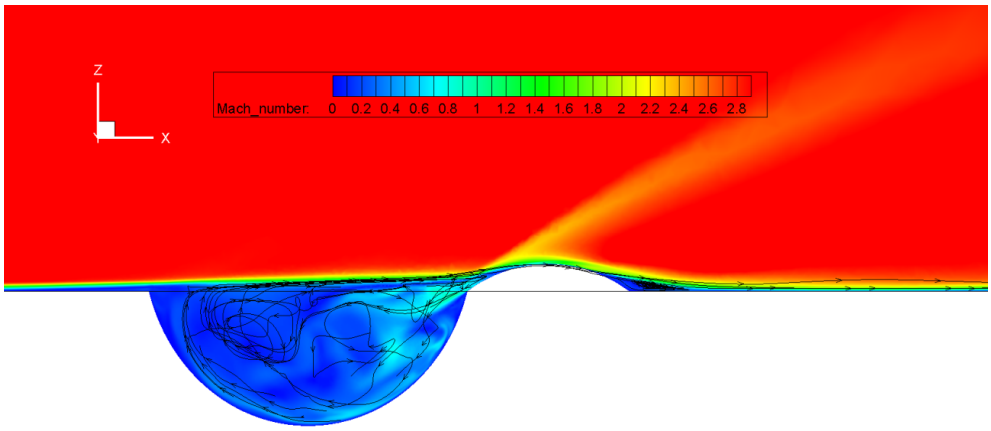

Figure 11. Mach number contour across the simulated hot perforation geometry (case 4).

4. CONCLUSION

With the presented experimental studies, the feasibility of high-power laser irradiation tests of various materials under subsonic and supersonic conditions with flow and exposure times up to 30 seconds were demonstrated. The results showed that the laser caused perforation of 5 mm thick representative missile materials within a few seconds in both a subsonic and supersonic flow. In general, the higher the laser power, the shorter the perforation time. For CFRP material, a minor correlation of the perforation times could be observed with respect to the applied flow conditions, i.e. the higher the flow velocity the faster the perforation. The perforation time of flat plates made of steel were shortened by a factor of three in subsonic and supersonic flow compared to the static environment. However, for aluminum no clear dependence of the perforation time on the flow speed in static, subsonic and supersonic conditions could be observed.

High-speed imaging illustrated the diverse process dynamics depending on the irradiated material. Among others, irradiating steel is associated with melting and the generation of sparks, while the laser induced decomposition and fiber fragmentation is typical for CFRP. The observed melting and ablation processes were further studied by means of a visual inspection of the damaged targets in order to determine the extent of damage like the heat-affected zones of CFRP composite structures or the shape of solidified molten material. Thermography was utilized to observe temperature profiles during laser irradiation and to correlate these signals with material changes like melting. Furthermore, the

accuracy of thermography could be further improved by implementing a temperature dependent emissivity or using another spectral range that is more applicable for the hot reaction of the composite materials. Schlieren imaging and numerical three-dimensional, steady and uncoupled simulations indicated that additional aerodynamic forces, caused by laser radiation damages, were not significant.

The established experimental environment and measurement instrumentation provided an initial overview of encountering effects of laser-material-aerodynamic interactions with respect to missile defense. It is planned, that in future studies the parameter range is extended, including hypersonic flows, to derive quantitative interdependencies of those effects.

REFERENCES

[1] Brockmann, K., Stefanovich, D., "Hypersonic boost-glide systems and hypersonic cruise missiles", SIPRI Stockholm (2022).

[2] Wortzel, L. M., "Hypersonic Weapons Development in China, Russia and the United States: Implications for American Security Policy", Land Warfare Paper No. 143, (2022).

[3] Abbas, S. B., "Hypersonic and Directed-Energy Weapons - A New Arms Race", International Relations Insights & Analysis, (2021)

[4] O'Keefe, J.D., Johnson, R. L., "Laser Burnthrough Time Reduction Due to Tangential Airflow - An Interpolation Formula", AIAA Journal, Vol. 12, (1974).

[5] Robin, J.E., Nordin, P., "Reduction of cw laser melt-through times in solid materials by transverse gas flow", Journal of Applied Physics 46, 2538 (1975).

[6] Crane, K.C.A., "Ablation of materials subjected to laserradiation and high-speed gas flows", Journal of Applied Physics 51, 5954 (1980).

[7] Baek, W. K., "Melt-through characteristics in continuous beam irradiation of flying metal samples in flow speeds up to 85 m/s", Optics & Laser Technology, Volume 45, Pages 250-255, (2013).

[8] Wei, C "Melt removal mechanism by transverse gas flow during laser irradiation," Proc. SPIE 10173, Fourth International Symposium on Laser Interaction with Matter, 1017303 (2017).

[9] Wang, J., "Experimental investigation on laser ablation of C/SiC composites subjected to supersonic airflow", Optics and Laser Technology, 113, 399-406, (2019)

[10] Zhao, W., "Effects of tangential supersonic airflow on the laser ablation of laminated CFRP", Journal of Materials Research and Technology, Vol. 14, 1985-1997, (2021).

[11] Wang et al., " Physics and Computation of Aero-Optics,", Annu. Rev. Fluid Mech Vol. 44:299-321, (2012).

[12] Wolfrum et al., "High-energy laser effects on carbon fiber reinforced polymer composites with a focus on perforation time", Journal of Composite Materials, Vol 55, Issue 16, (2021).

[13] Osterholz et al., "Experimental characterization of energy transfer from large-diameter kilowatt continuous-wave laser beams to metal samples", J. Laser Appl., 29, 012011 (2017).

[14] Schmücker et al., "Mesostructure of WHIPOX All Oxide Ceramics", High Temperature Ceramic Matrix Composites, Pages 670-674, (2001)

[15] Chanteloup, J.-C., "Multiple-wave lateral shearing interferometry for wave-front sensing", Appl. Opt. 44, 1559-1571 (2005)

[16] Allheily et al., "An experimental method to assess the thermo-mechanical damage of CFRP subjected to a highly energetic 1.07 μm-wavelength laser irradiation", Comp. Part B Eng., Volume 92, Pages 326-331, (2016).

[17] P M Reynolds, P. M., "Spectral emissivity of 99.7% aluminium between 200 and 540 °C", Br. J. Appl. Phys., 12, 111 (1961).

[18] Langer et. al., "The DLR Flow Solver TAU - Status and Recent Algorithmic Developments", AIAA 2014-0080, Solver Technology for Turbulent Flows I, (2014)

[19] Mack, A., Hannemann, V., "Validation of the Unstructured DLR-TAU-Code for Hypersonic Flows", 32nd AIAA Fluid Dynamics Conference and Exhibition; FD-14: CFD Verification, (2002)

[20] Menter, F. R., "Two-equation eddy-viscosity turbulence models for engineering applications", AIAA Journal, Vol. 32, No. 8, (1994)